Pharm Res (2014) 31:1450–1459
DOI 10.1007/s11095-013-1048-x

RESEARCH PAPER

In Vivo Investigation of Hybrid Paclitaxel Nanocrystals with Dual Fluorescent Probes for Cancer Theranostics

Christin P. Hollis • Heidi L. Weiss • B. Mark Evers • Richard A. Gemeinhart • Tonglei Li

Received: 5 December 2012 / Accepted: 2 April 2013 / Published online: 26 April 2013

ABSTRACT

Purpose To develop novel hybrid paclitaxel (PTX) nanocrystals, in which bioactivatable (MMPSense® 750 FAST) and near infrared (Flamma Fluor® FPR-648) fluorophores are physically incorporated, and to evaluate their anticancer efficacy and diagnostic properties in breast cancer xenograft murine model.

Methods The pure and hybrid paclitaxel nanocrystals were prepared by an anti-solvent method, and their physical properties were characterized. The tumor volume change and body weight change were evaluated to assess the treatment efficacy and toxicity. Bioimaging of treated mice was obtained non-invasively *in vivo*.

Results The released MMPSense molecules from the hybrid nanocrystals were activated by matrix metalloproteinases (MMPs) *in vivo*, similarly to the free MMPSense, demonstrating its ability to monitor cancer progression. Concurrently, the entrapped FPR-648 was imaged at a different wavelength. Furthermore, when administered at 20 mg/kg, the nanocrystal formulations exerted comparable efficacy as Taxol®, but with decreased toxicity.

Conclusions Hybrid nanocrystals that physically integrated two fluorophores were successfully prepared from solution. Hybrid nanocrystals were shown not only exerting antitumor activity, but also demonstrating the potential of multi-modular bioimaging for diagnostics.

KEY WORDS breast cancer · MMPSense · nanocrystals · paclitaxel · theranostics

ABBREVIATIONS

DLS	Dynamic light scattering
MMP	Matrix metalloproteinase
NIR	Near infrared
PBS	Phosphate buffered saline
PTX	Paclitaxel
SEM	Scanning electron microscope

INTRODUCTION

Cancer theranostics aim to deliver anticancer agents concurrently with diagnostic probes. Ideally, the integrated system permits the treatment of cancer and, at the same time, achieves the recognition, evaluation, and transmission of the disease state by probing tumor biomarkers or pathological conditions. It is equally important to allow real-time, non-invasive tracking of the tissue distribution and tumor accumulation of the treatment system. Any live feedback of the integrated construct can clearly be used to further optimize the delivery system with improved tumor-targeting efficacy and minimized toxicity. While any successful implementation of integrated systems to

C. P. Hollis
Department of Pharmaceutical Sciences, College of Pharmacy
University of Kentucky, Lexington, Kentucky 40536, USA

H. L. Weiss
Biostatistics, Division of Cancer Biostatistics, Markey Cancer Center
University of Kentucky, Lexington, Kentucky 40506, USA

B. M. Evers
Department of Surgery and Markey Cancer Center
University of Kentucky, Lexington, Kentucky 40506, USA

R. A. Gemeinhart
Departments of Biopharmaceutical Sciences, Bioengineering, and Ophthalmology and Visual Sciences University of Illinois
Chicago Illinois 60612, USA

T. Li (✉)
Department of Industrial and Physical Pharmacy, College of Pharmacy
Purdue University, Heine Pharmacy Building, 575 Stadium Mall Drive
West Lafayette, Indiana 47907-2091, USA
e-mail: tonglei@purdue.edu

diagnose and treat cancers may be years ahead, integrating bioimaging agents into a drug delivery system has been actively pursued and continued to be improved.

To be assembled together with a drug delivery system, an imaging probe is generally encapsulated in the core, physically adsorbed to the surface, or chemically conjugated to the encapsulating materials of the system. Amongst various delivery vehicles, liposomes (1), polymersomes (2), polymeric nanoparticles (3), and micelles (4), are commonly utilized for the construction of theranostic systems. For instance, theranostic liposomes were reported to be constructed by simultaneously integrating antineoplastic agents and bioimaging probes (e.g., quantum dots, gadolinium, and radionuclides) (1,5,6). Superparamagnetic iron oxide and doxorubicin were also embedded together into hybrid polymersomes (7), polymeric nanoparticles (8), and polymeric micelles (9). Nonetheless, many of the existing nano-encapsulation systems bear inherent limitations, including low drug loading capacity (4), complexity in the production (10), and vehicle toxicity (10).

A proof-of-concept study of a novel theranostic system has recently been conducted by our laboratory; the delivery system is of drug nanocrystals in which guest substances (e.g., fluorophores) are physically incorporated (11). The hybrid nanocrystals are formulated by a bottom-up, crystallization approach; no chemical conjugation is involved. Herein, to further evaluate the hybrid nanocrystal concept for cancer theranostics, we produced and tested paclitaxel (PTX) nanocrystals *in vivo* that concurrently incorporated two unique bioimaging fluorophores, bioactivatable MMPSense 750 FAST and near-infrared FPR-648. MMPSense 750 is a polymer where fluorophores are covalently linked to a polymeric backbone. The fluorophores are in the quenched state because of their close distances and become highly fluorescent when their linkage bonds are chemically cleaved by matrix metalloproteinases (MMPs). MMPs are a large family of zinc—dependent proteolytic enzymes, and MMP-2 (gelatinase-A) and MMP-9 (gelatinase-B) are known to be involved and overexpressed in the progression of many types of cancer (12–14). It is reported that MMPSense made it possible to correlate the fluorescence signal and the presence of pathologically confirmed colonic adenocarcinoma *in vivo* (15,16). The bioactivatable probe is highly sensitive and allows detection of a small number of pre-cancerous or cancerous cells with elevated MMP activities (15). The MMPSense 750 was expected to be activated by MMPs offering a live feedback of tumor progression, while the entrapped FPR-648 assisted in non-invasively tracing the biodistribution of the nanocrystals. Because their emission wavelengths are separated by 100 nm (MMPSense λ_{em}: 775 nm, FPR-648 λ_{em}: 672 nm), the fluorescent signals can be resolved by two separate excitation/emission windows.

In this report, preparation and characterization of pure PTX and hybrid PTX/MMPSense/FPR nanocrystals are first discussed. *In vivo* bioimaging of breast cancer-xenografted mice treated by the hybrid nanocrystals is then presented. Finally, the efficacy of anticancer treatment by the hybrid nanocrystals to the mice is examined and compared with the treatment by a conventional formulation, Taxol.

MATERIALS AND METHODS

Materials

PTX (>99.5% purity) was purchased from 21CECPharm (United Kingdom); FPR-648 fluorophore (λ_{ex}=648 nm; λ_{em}=672 nm) was obtained from Akina LLC (West Lafayette, IN); MMPSense FAST 750 (MW: ~ 43,000 g/mol; λ_{ex}=745 nm; λ_{em}=800 nm) was purchased from Perkin Elmer (Waltham, MA). Ethanol (HPLC grade), acetonitrile (HPLC grade), and DMSO (dimethyl sulfoxide, ACS grade) were purchased from Fisher Scientific (Pittsburgh, PA). All chemicals and solvents were utilized without further purification. Deionized water (by Milli-Q®, filtered through 0.2 μm membrane) was used for all experiments. 0.050 μm Whatman® Nuclepore polycarbonate track-etched membranes used for filtration were purchased from Fisher Scientific (Pittsburgh, PA). MCF-7 human breast adenocarcinoma cells were purchased from the American Type Culture Collection (ATCC).

Preparation of Pure and PTX/MMPSense/FPR Hybrid Nanocrystals

Pure and hybrid PTX nanocrystals were produced by an anti-solvent crystallization method. In general, to grow pure nanocrystals, 1 mL of PTX ethanol solution at 5 mg/mL was added to 20 mL deionized water in a round-bottom flask. The mixture was subjected to stirring and sonication (F20D, Fisher Scientific, Pittsburgh, PA) for 10 min. To grow hybrid PTX/MMPSense/FPR nanocrystals, 6.48 nmol (0.27 mL) of MMPSense 750 and 0.635 mg (0.127 mL) of FPR-648 were added to deionized water prior to the addition of PTX solution; the solution was then stirred and sonicated. After crystallization, the solution was filtered through a 50-nm polycarbonate membrane, and the retentate was re-suspended in water for additional filtration-re-suspension cycles to remove loosely bounded imaging agents on the surface of nanocrystals.

Physical Characterization and Chemical Analysis of Nanocrystal Systems

Scanning electron micrographs were obtained with a Hitachi SEM 4300 (Hitachi High Technologies America, Inc., Schaumburg, IL) at accelerating voltage of 3 kV. Samples were sputter coated with gold palladium (Au/Pd) for 1 min

under a current of 20 mA. The longest dimension of nanoparticles was measured from obtained SEM images by SigmaScan (Systat software, San Jose, CA), and the mean plus or minus the standard deviation (± S.D.) of approximately 100 particles was calculated. The hydrodynamic diameter, polydispersity index, and zeta potential were measured in deionized water using a dynamic light scattering (DLS) system (Malvern Zetasizer, Nano-ZS, Worcestershire, United Kingdom). Measurements were performed in triplicate.

PTX concentrations were analyzed by a high-performance liquid chromatography (HPLC) system (Waters Breeze with a dual wavelength absorbance detector, Waters 2487, Milford, MA) at an absorbance wavelength of 227 nm. A reverse-phase C-18 column (5 μm, 150 mm × 4.6 mm, Waters) was used. The mobile phase composed of 50% acetonitrile and 50% deionized water was pumped at a flow rate of 2 mL/min. Column was equilibrated to 35°C prior to sample injection (20 μL). Small aliquots of paclitaxel nanocrystals were dissolved in ethanol prior to the HPLC analysis (done in triplicate).

IVIS Spectrum (Perkin Elmer, Waltham, MA) was utilized to measure the percent entrapment of fluorophores (MMPSense 750 and FPR-648, respectively) in the hybrid nanocrystals by dissolving small aliquot in DMSO. Standard solutions of MMPSense 750 and FPR-648 were prepared in DMSO; MMPSense was completely cleaved and unquenched in DMSO. Standards and dissolved hybrid nanocrystals were placed in 96-well plates prior to analysis under IVIS Spectrum®. Samples were prepared in triplicate. MMPSense 750 standards were prepared at concentrations of 0.2, 0.5, 1, and 2 nmol/mL, while those of FPR-648 were at concentrations of 0.25, 0.5, 0.75, and 1 μg/mL. MMPSense 750 was analyzed at excitation and emission wavelengths of 745 and 800 nm, respectively, while FPR-648 was analyzed at lower wavelengths ($\lambda_{excitation}$: 640 nm, $\lambda_{emission}$: 700 nm). The standard solutions and samples were placed in a 96-well plate, and the fluorescence intensities from the individual wells were analyzed by Living Image software 4.2 (Perkin Elmer, Waltham, PA). A standard curve was then obtained from the fluorescence intensity measured by IVIS *versus* concentration and used for calculating the fluorophore concentration in the hybrid nanocrystals.

Cell Culture of MCF-7

MCF-7 human breast adenocarcinoma cells were cultured in Dulbecco's Modified Eagle Medium (DMEM, Hyclone) supplemented with 10% fetal bovine serum (Hyclone) and 1% penicillin/streptomycin (Hyclone). Trypsin-ethylenediaminetetraacetic acid (Trypsin-EDTA, Mediatech) was used to dissociate cells from a culture dish. All of the cell culture reagents were purchased from Fisher Scientific (Pittsburgh, PA). Cells were cultured at 37°C in a humidified atmosphere with 5% CO_2. To establish the MCF-7 xenograft in nude mice, cells were harvested (by using 0.25% trypsin-EDTA) when they were 70–90% confluent. After being counted, cells were suspended in serum-free DMEM at concentration of 5×10^7 cells/mL and kept in an ice bucket prior to their inoculation.

Animal Model

Female nude outbred mice (Tac:Cr: (NCr)-Foxn1 Nu) were obtained from Taconic at 4 weeks of age (14–20 g). All of the animal experiments complied with the principles of care and use of laboratory animals and were approved by the University of Kentucky Institutional Animal Care and Use Committee (IACUC). Seven days after arrival, one 17*β*-estradiol pellet (1.7 mg, 60-day release; Innovative Research of America, Inc.) was implanted under the skin between the ears of each mouse. Two days later, 5×10^6 MCF-7 cells (100 μL) were inoculated subcutaneously into each side of the mammary fat pad. All experimental procedures were performed under general anesthesia by isoflurane inhalation. Tumor growth and metastatic potential are heavily affected by the site of inoculation (17–20). 17β-estradiol pellets were used to encourage metastasis of MCF-7 as it was reported that metastases appeared within 5–7 weeks following MCF-7 subcutaneous inoculation to the mammary fat at frequency of 40–60% (21). Subsequent to the treatment injections, animals were monitored daily for their body weight and tumor volume using a digital caliper. The tumor volume (TV) was calculated by using the following equation: $TV = \text{longest dimension} \times (\text{shortest dimension})^2/2$.

Table I Animal Groups That Received Intravenous Injections

Group	Number of mice	Paclitaxel dose	MMPSense
No xenograft	5	–	0.1 nmol
No treatment	6	–	0.1 nmol
Taxol	6	20 mg/kg	0.1 nmol
PTX nanocrystals	6	20 mg/kg	0.1 nmol
PTX/MMPSense/FPR nanocrystals	6	20 mg/kg	0.2 nmol

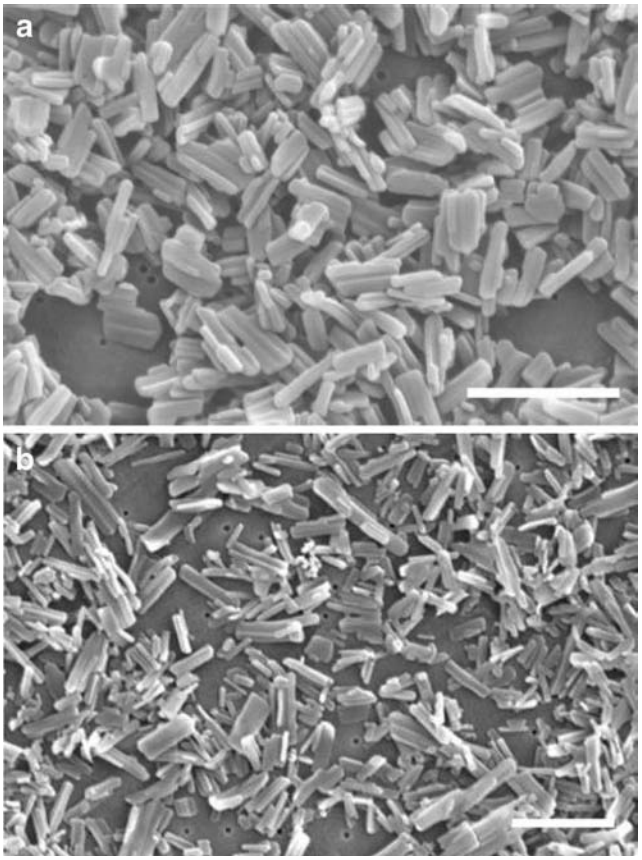

Fig. 1 SEM images of PTX (**a**) and PTX/MMPSense/FPR-648 nanocrystals (**b**). Scale bars represent 1 μm.

Approximately 8 weeks after tumor inoculation, a total of 24 mice were randomized into 4 groups (n=6): (a) no treatment (control), (b) Taxol treatment, (c) PTX nanocrystal treatment, and (d) PTX/MMPSense/FPR hybrid nanocrystal treatment. Taxol formulation was prepared by diluting 0.3 mL of 30 mg/mL of paclitaxel in Cremophore EL/ethanol (50:50) solution with 2.7 mL of saline (0.9% sodium chloride). Intravenous injections that were administered on day 0 to the mice *via* tail veins were summarized in Table I. Mice in the untreated group received 0.1 nmol of the bioactivatable dye, MMPSense 750. The Taxol and PTX nanocrystals groups received an equivalent dose of 20 mg/kg PTX plus 0.1 nmol MMPSense 750. Meanwhile, the PTX hybrid nanocrystal group received the same dose of 20 mg/kg PTX with 0.2 nmol of MMPSense 750 entrapped in the drug nanocrystals. The *in vivo* performance of the free and entrapped MMPSense 750 in hybrid nanocrystals were monitored by the IVIS Spectrum (at λ_{ex}: 745 nm, λ_{em}: 800 nm). The fluorescence signal of the entrapped FPR-648 in PTX/MMPSense/FPR hybrid nanocrystals was also longitudinally monitored by the IVIS at λ_{ex}: 640 nm, λ_{em}: 700 nm.

Bioimaging

The animals were anesthetized by isoflurane inhalation during the IVIS imaging. Images were all taken with the same parameters as follows: (a) exposure time: 4 s for MMPSense 750 and 0.25 s for FPR-648, (b) F/Stop: 2, (c) binning: 8 (medium), (d) field of view (FOV): 13. All mice were euthanized at day 7. Their tumor volume and body weight were measured daily subsequent to the intravenous injection. The mean and standard deviation of fluorescent signal intensities were quantified by Living Image 4.2 software (Perkin Elmer, Waltham, MA).

Statistical Analysis

Graphical displays of the percent change in body weight were generated for each treatment group. Pairwise comparisons at each time point of follow-up were performed using the non-parametric Wilcoxon rank-sum test to account for non-normality of the data. The percent change in tumor volume at specific time points was compared between groups by an analysis of variance model with pairwise comparisons between groups generated from the model.

RESULTS AND DISCUSSION

Characterization of PTX Pure and PTX/MMPSense/FPR Hybrid Nanocrystals

The PTX nanocrystals, both pure and hybrid, were produced by the anti-solvent crystallization method from solution (Fig. 1). Particle size, polydispersity index, and zeta potential of both products are listed in Table II. Due to an extended period of stirring of 30 min, which encouraged further crystal growth and guest entrapment, the PTX hybrid nanocrystals had a larger mean particle size relative to

Table II Physical Properties of PTX Pure and Hybrid Nanocrystals (Mean ± S.D.)

Properties	PTX nanocrystals	PTX/MMPSense/FPR nanocrystals
Particle size (nm)	300 ± 140	380 ± 140
Hydrodynamic diameter (nm)	270 ± 5	282 ± 21
Polydispersity index	0.10 ± 0.03	0.19 ± 0.05
Surface charge (mV)	−14.9 ± 0.1	−20.6 ± 0.6

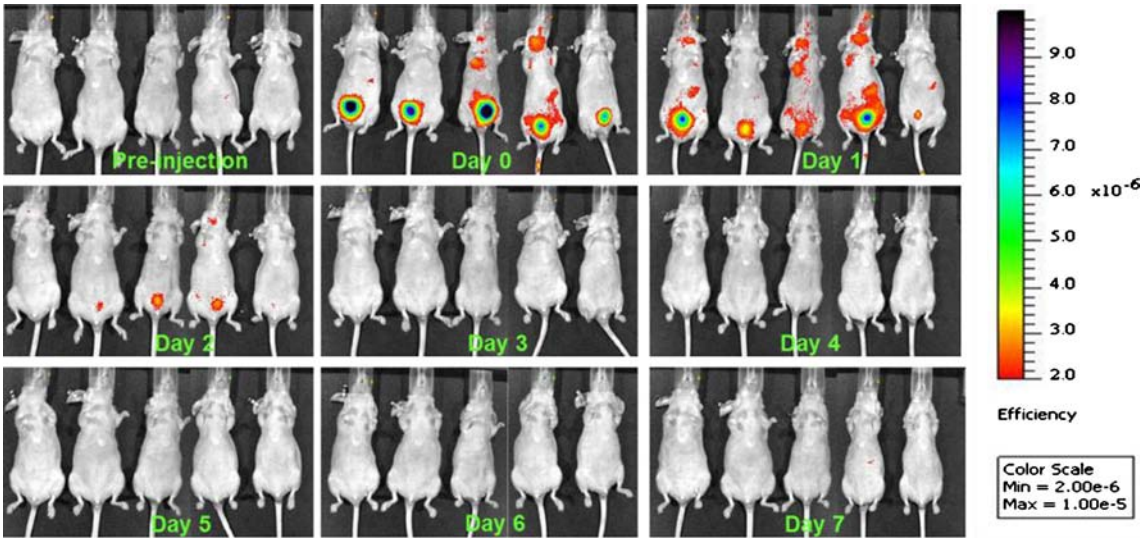

Fig. 2 IVIS images of non-xenografted mice ($n = 5$) injected with 0.1 nmol MMPSense 750 in PBS.

that of the pure PTX ($p < 0.001$). The hydrodynamic diameter of the pure nanocrystals determined from DLS was similar to the particle size analyzed from the SEM images. In contrast, the particle size of the PTX/MMPSense/FPR nanocrystals determined by DLS was underestimated possibly because of their elongated shape and particle size heterogeneity. The polydispersity indices suggest that the size distribution of the pure PTX nanocrystals was narrower than that of the PTX hybrid nanocrystals. In addition, the more negative value of zeta potential of the hybrid nanocrystalsis suspected due to the adsorption of MMPSense molecules, which are negatively charged in the aqueous environment (according to the manufacturer). Although the exact molecular structure of MMPSense is undisclosed, the technology was based on the bioactivatable probes previously reported (22). The polymer backbone, which supports the cleavable site (proline-leucine-glycine-valine-arginine peptide) and unquenched fluorophores (23), could promote higher adsorption of MMPSense to the surface of the nanocrystals, in addition to being integrated in the crystal lattice.

The amounts of the integrated fluorophores were analyzed by the IVIS Spectrum. The standard curves were generated from triplicate standard solutions of MMPSense 750 and FPR-648 in DMSO; the R^2 values of the standard curves were 0.991 and 0.998 for MMPSense and FPR-648, respectively. It was then determined that there were 1.6 nmol/mL of MMPSense 750 relative to 3.76 mg/mL of PTX nanocrystals,

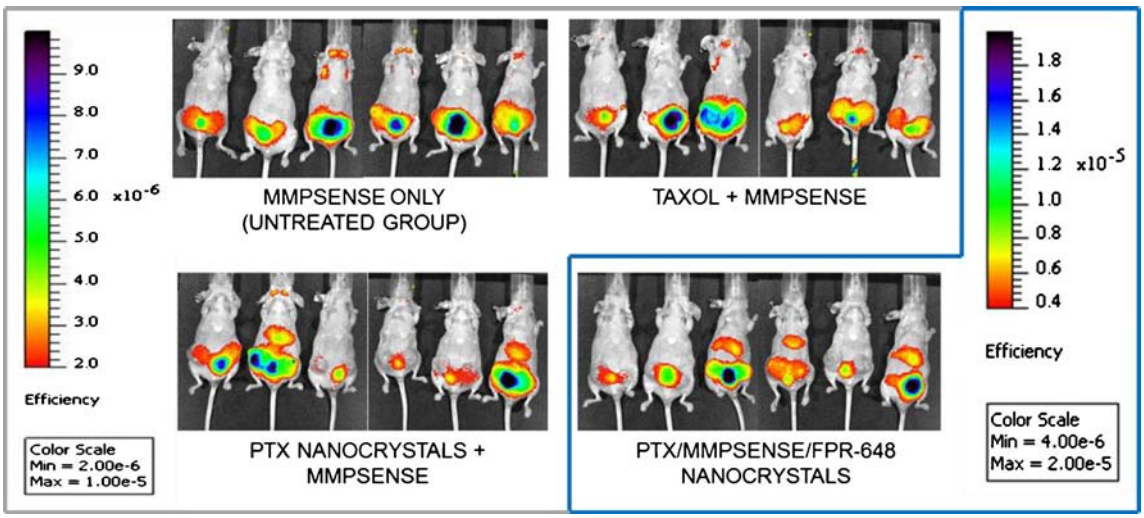

Fig. 3 IVIS images of mice from different treatment groups at day 2 after injection. MMPSense solution (0.1 nmol) was given to the first three groups with or without the treatment, while approximately 0.2 nmol of MMPSense were entrapped in the injected hybrid nanocrystals given to the last group. The color intensity scale was doubled (4×10^{-6} to 2×10^{-5}) of the last group in order to match the half amount of the dyes used in the first three groups (2×10^{-6} to 1×10^{-5}).

giving the percent entrapment of 1.83% (w/w); there were also 0.5 μg/mL of FPR-648, giving the percent entrapment of 0.01% (w/w).

Fluorescence Imaging of MMPSense 750 *In Vivo*

The ability of PTX hybrid nanocrystals as a theranostic system was evaluated in a mouse xenograft human breast cancer, MCF-7, model. First, 0.1 nmol of the MMPSense 750 dissolved in phosphate buffered saline (PBS) was injected into athymic mice without any tumor burden, and the animals were imaged by IVIS (Fig. 2). Because no tumor was initiated in the animals and MMPs were minimally expressed, little fluorescent signal should have been observed. Nonetheless, fluorescent signals were detected up to day 2 after the injection. It was later confirmed with the supplier that the dye was not 100% quenched (or conjugated), i.e., mixed with a small percentage of unquenched fluorophores due to the synthesis process. At day 2, most of the unquenched dye was renally cleared from the body.

PTX hybrid nanocrystals were given to tumor-bearing mice at 20 mg/kg, which led to the amount of the entrapped MMPSense equivalent to 0.2 nmol per animal. To validate and compare the bioactivated fluorescence bioimaging by the entrapped and free dye, 0.1 nmol (due to the availability, which is half of the amount of the entrapped dye) of the free MMPSense (in PBS) was injected simultaneously with Taxol, pure PTX nanocrystals, or by itself to the respective

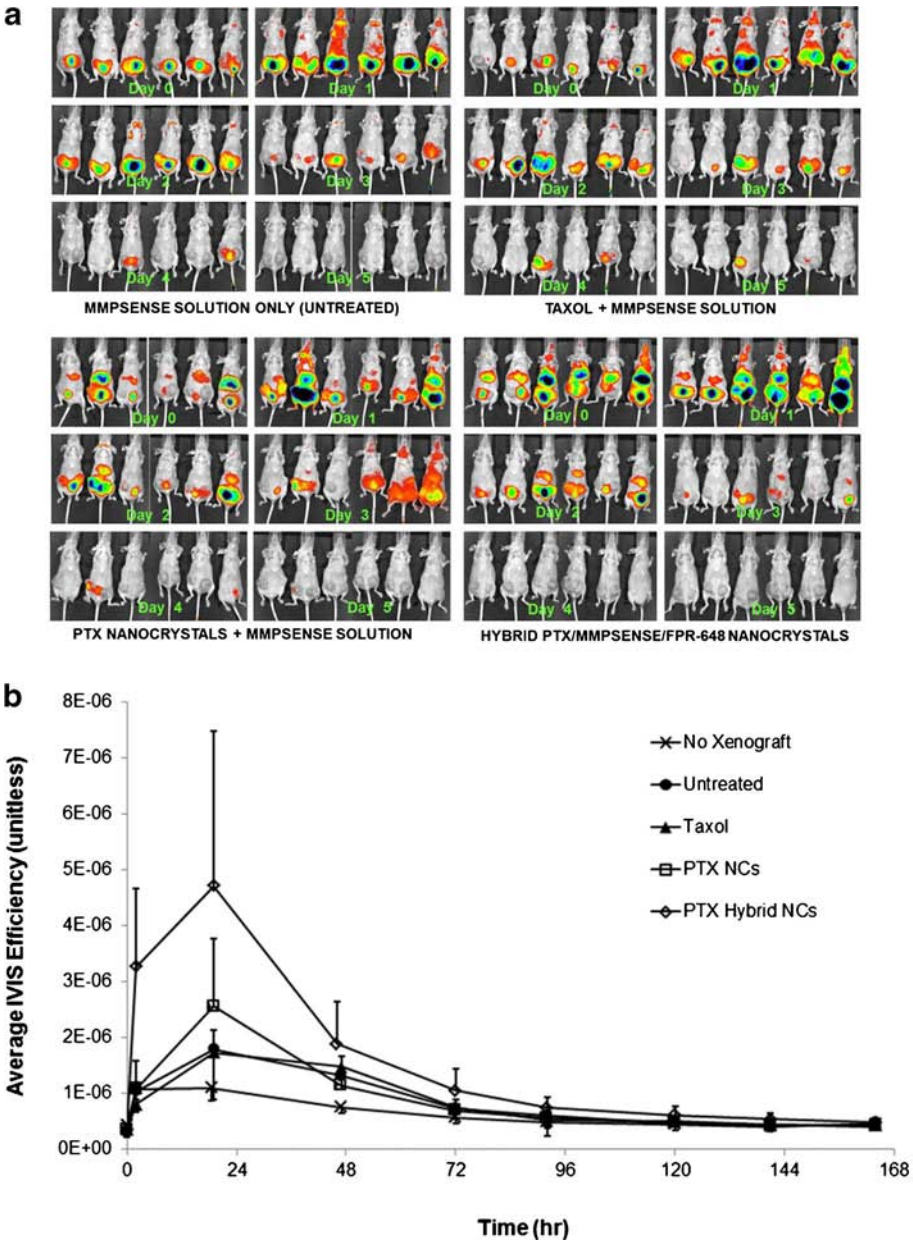

Fig. 4 (**a**) IVIS images of mice from untreated, Taxol, PTX pure, and PTX hybrid nanocrystal groups from day 0 to day 5. Day 0 images were taken 2 h post-injection. The color scale from the PTX hybrid nanocrystal group (*left*) was doubled compared to the other groups (as in Fig. 3). (**b**) The average IVIS efficiency (i.e., IVIS efficiency (cm^2) divided by the area of each mouse (cm^2)) was plotted against the time. The data points indicate mean ± S.D. $n = 6$ for the xenografted mice (Fig. 4a) and $n = 5$ for no-xenograft group (Fig. 2).

animal groups (Table I). IVIS images were obtained from the four groups. Figure 3 shows the images at day 2 when the majority of the pre-existing unquenched MMPSense had been cleared. The apparent fluorescence signals at day 2, hence, should signify the intensities that were due to MMPSense activation. The cleaved fluorophores, which are hydrophilic, were then cleared renally. Due to the difference in the chemical makeup, the clearance of the paclitaxel may differ from the fluorophores. Apparently, the entrapped MMPSense in the PTX hybrid nanocrystals was capable of exerting the same functionality to respond to the elevation of MMPs as that by the unbound MMPSense. This suggests that the entrapped MMPSense dyes were released out of the nanocrystals and cleaved by MMPs in the main tumor and metastasis sites.

The IVIS images of mice from all the treatment groups from day 0 to 5 are summarized in Fig. 4a. The mean and standard deviation of fluorescent signal intensities are shown in Fig. 4b. Based on Fig. 4a (day 0 to 3 images), stronger fluorescent signals observed in some mice of the pure and hybrid nanocrystal groups may arise from the variation in the amount of MMPSense in the intravenous injection. The mice showing stronger signals in later time points had higher initial intensities on day 0. Furthermore, although some degrees of variation were observed, the mean values of the photonic efficiency from all of the xenografted mice were almost doubled at 19 h after the injection (Fig. 4b). Compared with the signal decrease observed in the mice with no xenograft, the signal amplification in the xenografted mice signified that the MMPSense probe was activated by the MMPs. It is also worth noting that the MMPSense incorporated in the hybrid nanocrystals were able to perform similarly to the free MMPSense, which was injected by itself (for the untreated group) or along with other treatments (Taxol and pure paclitaxel nanocrystals). The large standard deviation in the hybrid nanocrystal group was caused by the variability on the amount of MMPSense, both integrated and on the surface of the nanocrystals, in each injection. Figure 4a further suggests that there were more unquenched dyes integrated with the nanocrystals, likely resulting from the integrity of MMPSense being compromised due to the exposure to ethanol, rapid stirring, and intense sonication during the process of nanocrystal production. The unquenched dyes were mostly cleared before day 2 through the kidney and urinary bladder, and most of the fluorescence imaging observed on day 2 should have arisen from the quenched dyes that were released from the nanocrystals and cleaved by the MMPs. In all groups, the fluorescence signals died down significantly after day 3. While nanocrystals are believed to slowly dissolve and survive longer than a few days, the similarity in the fluorescence imaging by the two groups did imply the possibility that MMPSense molecules were mostly adsorbed to the surface of the hybrid nanocrystals, detached quickly upon the injection of the nanocrystals. Because the chemical nature of the dye molecule remains undisclosed, it can only be speculated that the large molecule may be amphiphilic, surfactant-like. Moreover, given the relatively large entrapment ratio

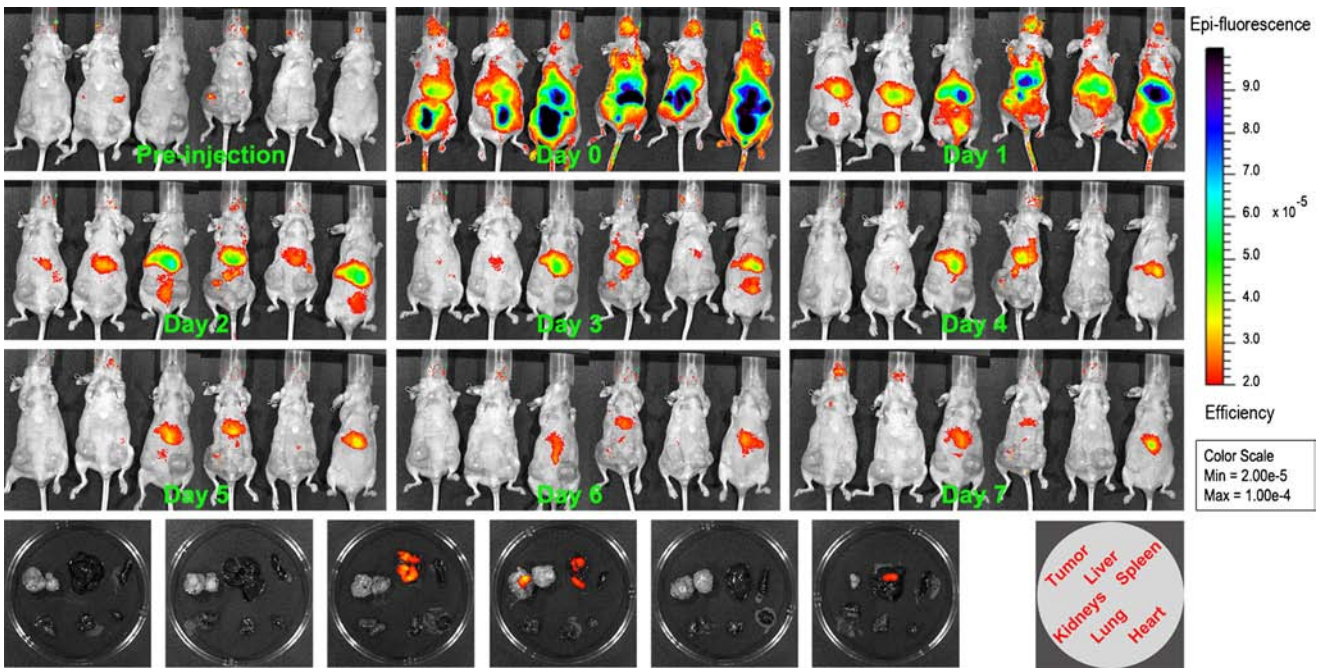

Fig. 5 IVIS images of mice in the hybrid nanocrystal group obtained at the 700-nm emission wavelength. The excised tumors and major organs (liver, spleen, kidneys, lung, and heart) were imaged on day 7 with the same imaging parameters.

(1.83% w/w), a majority of the dyes were more likely not integrated throughout the nanocrystals, differing from FPR-648 discussed below.

Fluorescence Imaging of FPR-648 *In Vivo*

In order to non-invasively trace the biodistribution of drug nanocrystals in real-time and *in vivo*, it was intended to incorporate the NIR dye FPR-648 in the crystal lattice of the nanocrystals. IVIS images of mice treated by the PTX/MMPSense/FPR nanocrystals were obtained at the lower emission wavelength (Fig. 5). The slightly fluorescent spots obtained from the animals prior to the injection were due to the autofluorescence. Subsequent to the intravenous injection, the fluorescence imaging of FPR-648 indicates that a majority of the hybrid nanocrystals were accumulated in the liver. Because of their size range, 250–550 nm, the hybrid nanocrystals were prone to be sequestered by the Kupffer cells in the mononuclear phagocyte system (MPS). It is important to note that the observed fluorescence arose from the combination of both entrapped and dissolved dye molecules. In our earlier study, the solution of another NIR dye, which has similar chemical structure to FPR-648, was cleared approximately 72 h subsequent to the injection (11). Thus, given the fact that the fluorescence remained up to day 7, it is highly plausible that the nanocrystals were not completely dissolved or cleaved, continuously releasing the dye molecules. It is thus suggestive that PTX molecules may be released from the hybrid nanocrystals accumulated in the liver re-entering the blood circulation. From the bioimaging of excised tumor and major organs (Fig. 5), the liver emitted the strongest fluorescence and the tumor also bore residual signals. The imaging results differ from our earlier data where the tumor showed the strongest intensity (11). Note that only one NIR dye was integrated in the PTX nanocrystals in the earlier study (11); the integration and possibly surface adsorption of the large, negatively charged molecules, MMPSense, altered the surface properties (e.g., surface charge and wettability) and possibly the biodistribution of the hybrid nanocrystals, compared with the PTX/FPR-749 nanocrystals

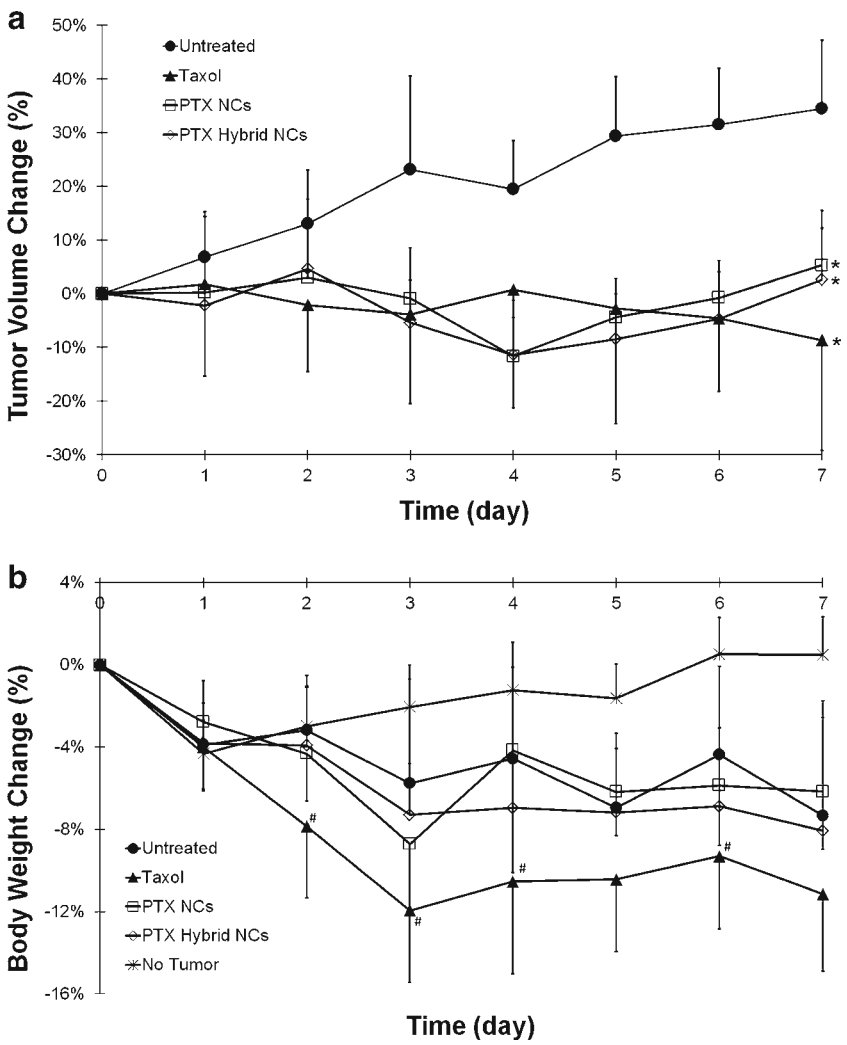

Fig. 6 (**a**) Percent change in tumor volume measured daily after single injection of respective treatments (Taxol, PTX nanocrystals, and PTX hybrid nanocrystals) on day 0. Each point indicates the mean ± S.D. ($n = 6$). * $P < 0.01$ compared to the untreated group on day 7. All treatments induced tumor suppression ($P < 0.05$) on days 3, 4, 5, and 6. (**b**) Percent change in body weight measured daily. Each point indicates the mean ± S.D. ($n = 6$). # $P < 0.05$ compared to the untreated group on days 2, 3, 4, and 6.

(11). From the theranostic point of view, the bioimaging results do support a great potential of the hybrid nanocrystals whose distribution can be traced in the real-time. Still, it is worth pointing out that the live fluorescence imaging that is measured is contributed by both integrated and unbound dye molecules. More importantly, the biodistribution of free dyes may be significantly different from that of drug molecules and/or nanocrystals. Further studies are clearly needed to resolve and fine-tune fluorescence imaging to trace the drug.

Treatment Efficacy and Toxicity

The anticancer efficacy by the nanocrystals was evaluated from the decrease in tumor volume. Compared with the untreated group, all of the treatments (Taxol, PTX nanocrystals, and PTX hybrid nanocrystals) induced tumor suppression ($p<0.05$) starting on day 3 after injection and continuing to day 7 (Fig. 6a). On day 7, the treatments significantly suppressed the tumor growth compared with the control group ($p<0.01$ for all treatments). There was no significant difference in the percent of tumor volume change among the treatments ($p>0.1$) throughout the study. Clearly, without any solubilization means, the nanocrystals were capable of inducing the same degree of tumor growth suppression as the solution formulation.

Furthermore, the treatment toxicity was evaluated by the percent body weight change during the course of the study (Fig. 6b). Note that all of the mice, including the ones without tumor burden, experienced some extent of body weight loss from daily transportation and exposure of anesthesia during the IVIS imaging process. Still, compared with the untreated group, the body weight decrease of the Taxol treated group was significantly greater ($p<0.05$) on days 2, 3, 4, and 6, and trends toward significance were observed on day 5 ($p=0.07$) and 7 ($p=0.16$). The mice in the Taxol treated group were able to recoup their body weight back by day 7 because most of the treatments might have been cleared following the single injection (24). Conversely, the body weights of mice in the pure and hybrid nanocrystal groups were not significantly different ($p>0.1$) from the control (untreated). The results indicate that nanocrystals were able to offer safer and less toxic delivery than the solubilized formulation. As such, it is possible to increase the dose of nanocrystals and achieve a more effective treatment.

CONCLUSIONS

In this study, the potential of paclitaxel hybrid nanocrystals as a cancer theranostic system was evaluated. Two imaging probes, MMPSense 750 and FPR-648, were intended to be physically incorporated in the drug nanocrystals that were formulated by crystallization. Both dyes were imaged at different excitation and emission wavelengths. While MMPSense reported the degree of metastasis, the integrated FPR-648 served as a tracer for the biodistribution of the nanocrystals in the animals. At a dose level of 20 mg/kg, PTX pure and hybrid nanocrystals were as efficacious as Taxol in suppressing the growth of MCF-7 xenograft. Yet, the nanocrystals induced less toxicity than the conventional solubilized formulation. The bioimaging capability of the hybrid nanocrystals was limited by the size and impurities of MMPSense. Despite the likeliness that MMPSense molecules may mostly adsorbed to the crystal surface, the study demonstrates that hybrid nanocrystals have a great potential to be utilized as a simple, versatile, and enabling platform for cancer theranostics. Studies are under way to explore other types of bioimaging modalities, using smaller and purer dyes, which are compatible with crystal integration. Furthermore, to have a better understanding of the optical imaging and the release of the optical dyes from nanocrystals, the biodistribution of nanocrystals, free drug, and dye molecules will be further investigated.

ACKNOWLEDGMENTS AND DISCLOSURES

The project described was supported by Grant Number R25CA153954 from the National Cancer Institute. The content is solely the responsibility of the authors and does not necessarily represent the official views of the National Cancer Institute or the National Institutes of Health.

REFERENCES

1. Al-Jamal WT, Kostarelos K. Liposomes: from a clinically established drug delivery system to a nanoparticle platform for theranostic nanomedicine. Acc Chem Res. 2011;44:1094–104.
2. Levine DH, Ghoroghchian PP, Freudenberg J, Zhang G, Therien MJ, Greene MI, *et al.* Polymersomes: a new multi-functional tool for cancer diagnosis and therapy. Methods. 2008;46:25–32.
3. Caldorera-Moore ME, Liechty WB, Peppas NA. Responsive theranostic systems: integration of diagnostic imaging agents and responsive controlled release drug delivery carriers. Acc Chem Res. 2011;44:1061–70.
4. Blanco E, Kessinger CW, Sumer BD, Gao J. Multifunctional micellar nanomedicine for cancer therapy. Exp Biol Med. 2009;234:123–31.
5. Weng KC, Noble CO, Papahadjopoulos-Sternberg B, Chen FF, Drummond DC, Kirpotin DB, *et al.* Targeted tumor cell internalization and imaging of multifunctional quantum dot-conjugated immunoliposomes *in vitro* and *in vivo*. Nano Lett. 2008;8:2851–7.
6. Li S, Goins B, Zhang L, Bao A. Novel multifunctional theranostic liposome drug delivery system: construction, characterization, and multimodality MR, near-infrared fluorescent, and nuclear imaging. Bioconjug Chem. 2012;23:1322–32.
7. Sanson C, Diou O, Thévenot J, Ibarboure E, Soum A, Brûlet A, *et al.* Doxorubicin loaded magnetic polymersomes: theranostic

nanocarriers for MR imaging and magneto-chemotherapy. ACS Nano. 2011;5:1122–40.
8. Maeng JH, Lee D-H, Jung KH, Bae Y-H, Park I-S, Jeong S, *et al.* Multifunctional doxorubicin loaded superparamagnetic iron oxide nanoparticles for chemotherapy and magnetic resonance imaging in liver cancer. Biomaterials. 2010;31:4995–5006.
9. Guthi JS, Yang SG, Huang G, Li SZ, Khemtong C, Kessinger CW, *et al.* MRI-visible micellar nanomedicine for targeted drug delivery to lung cancer cells. Mol Pharm. 2010;7:32–40.
10. Janib SM, Moses AS, MacKay JA. Imaging and drug delivery using theranostic nanoparticles. Adv Drug Deliv Rev. 2010;62:1052–63.
11. Zhao RS, Hollis CP, Zhang H, Sun LL, Gemeinhart RA, Li TL. Hybrid nanocrystals: achieving concurrent therapeutic and bioimaging functionalities toward solid tumors. Mol Pharm. 2011;8:1985–91.
12. Singer CF, Kronsteiner N, Marton E, Kubista M, Cullen KJ, Hirtenlehner K, *et al.* MMP-2 and MMP-9 expression in breast cancer-derived human fibroblasts is differentially regulated by stromal-epithelial interactions. Breast Cancer Res Treat. 2002;72:69–77.
13. Poulsom R, Hanby AM, Pignatelli M, Jeffery RE, Longcroft JM, Rogers L, *et al.* Expression of gelatinase A and TIMP-2 mRNAs in desmoplastic fibroblasts in both mammary carcinomas and basal cell carcinomas of the skin. J Clin Pathol. 1993;46:429–36.
14. Iwata H, Kobayashi S, Iwase H, Masaoka A, Fujimoto N, Okada Y. Production of matrix metalloproteinases and tissue inhibitors of metalloproteinases in human breast carcinomas. Jpn J Cancer Res: Gann. 1996;87:602–11.
15. Clapper ML, Hensley HH, Chang WC, Devarajan K, Nguyen MT, Cooper HS. Detection of colorectal adenomas using a bioactivatable probe specific for matrix metalloproteinase activity. Neoplasia. 2011;13:685–91.
16. Vartakand DG, Gemeinhart RA. Matrix metalloproteases: underutilized targets for drug delivery. J Drug Target. 2007;15:1–20.
17. Kozlowski JM, Fidler IJ, Campbell D, Xu ZL, Kaighn ME, Hart IR. Metastatic behavior of human-tumor cell-lines grown in the nude-mouse. Cancer Res. 1984;44:3522–9.
18. Meyvisch C. Influence of implantation site on formation of metastases. Cancer Metastasis Rev. 1983;2:295–306.
19. Morikawa K, Walker SM, Nakajima M, Pathak S, Jessup JM, Fidler IJ. Influence of organ environment on the growth, selection, and metastasis of human-colon carcinoma-cells in nude-mice. Cancer Res. 1988;48:6863–71.
20. Volpeand JPG, Milas L. Influence of tumor-transplatation methods on tumor-growth rate and metastatic potential of solitary tumors derived from metastases. Clin Exp Metastasis. 1990;8:381–9.
21. Shafieand SM, Liotta LA. Formation of metastasis by human breast carcinoma cells (MCF-7) in nude mice. Cancer Lett. 1980;11:81–7.
22. Weissleder R, Tung CH, Mahmood U, Bogdanov A. *In vivo* imaging of tumors with protease-activated near-infrared fluorescent probes. Nat Biotechnol. 1999;17:375–8.
23. Groves K, Kossodo S, Handy E, Jensen J, Blusztajn A, Cuneo G, *et al. In vivo* imaging of treatment effects using a novel near infrared labeled agent: MMPSense™ 750 FAST, AACR Annual Meeting, Denver, 2009.
24. Sparreboom A, van Tellingen O, Nooijen WJ, Beijnen JH. Nonlinear pharmacokinetics of paclitaxel in mice results from the pharmaceutical vehicle Cremophor EL. Cancer Res. 1996;56:2112–5.